

Multiscale Lagrangian Fluid Dynamics Simulation for Polymeric Fluid

Takahiro Murashima^{1,2*} and Takashi Taniguchi^{1,2†}

¹*Department of Chemical Engineering,
Kyoto University, Kyoto 615-8510, Japan*

²*CREST, JST, Kawaguchi, Saitama 332-0012, Japan*

(Dated: March 31, 2022)

Abstract

We have developed a simulation technique of multiscale Lagrangian fluid dynamics to tackle hierarchical problems relating to historical dependency of polymeric fluid. We investigate flow dynamics of dilute polymeric fluid by using the multiscale simulation approach incorporating Lagrangian particle fluid dynamics technique (the modified smoothed particle hydrodynamics) with stochastic coarse-grained polymer simulators (the dumbbell model). We have confirmed that our approach is nicely in agreement with the macroscopic results obtained by a constitutive equation corresponding to the dumbbell model, and observed microscopic thermal fluctuation appears in macroscopic fluid dynamics as dispersion phenomena.

PACS numbers: 47.11.St, 47.50.-d, 83.10.Ff, 83.10.Gr, 83.10.Mj, 83.50.Ha

Keywords: Multiscale simulation, Polymer rheology, CONNFFESSIT, Lagrangian fluid dynamics

*Electronic address: murasima@cheme.kyoto-u.ac.jp

†Electronic address: taniguch@cheme.kyoto-u.ac.jp

I. INTRODUCTION

Polymer rheology is complicated and exhibits various phenomena, e.g. vortex growth, die swell, or Weissenberg effect, caused by a collaboration between microscopic dynamics of polymers and macroscopic fluid dynamics[1]. In order to investigate such complex fluids, we usually take either one of the following two approaches[2]. One is a fluid dynamics approach regarding whole system as a continuum from a macroscopic viewpoint, and the other is a molecular dynamics approach from a microscopic viewpoint. Although there is a significant difference among applicable time and lengths scale in these approaches, we can improve our comprehension of polymer rheology from the intercommunication between the different hierarchies through parameters in constitutive equations. A lot of constitutive equations have been proposed to investigate variety of polymer rheology, but they are not always applicable to any kinds of polymeric liquids and the generalization of them is a considerably difficult issue. Then, in order to treat more general polymer rheology, an available approach is to incorporate the fluid dynamics approach directly with the molecular dynamics approach without constitutive equations. CONNFESSIT (Calculation of Non-Newtonian Flow: Finite Elements and Stochastic Simulation Technique) proposed by Laso and Öttinger[3] is one of the hierarchical approaches without assuming constitutive equations, and is a pioneer work in the multiscale simulation field, communicating with macroscopic finite elements and microscopic ensembles of polymers. However, it is an extremely heavy technique due to remeshing process in the finite element method to solve macroscopic fluid dynamics. After updating the displacements of particles holding microscopic ensembles of polymers, it is needed to remesh the finite elements in order to preserve one-to-one correspondence between macroscopic elements and microscopic particles representing the center of mass of ensembles. To avoid the difficulty of remeshing, a semi-Lagrangian approach[4] has been produced, where the convection terms are treated using a finite volume scheme, although this technique is acceptable only when the local stress does not depend on the history of flow. The heterogeneous multiscale method with the fully Eulerian approach at macroscopic level[5, 6] is sufficiently practical when we consider historically independent fluids, e.g. simple fluids, or Newtonian fluids.

In order to treat historical dependency associating with deformations and orientations of polymer coils and their entanglements, we develop a fully Lagrangian multiscale simulation

method, in which fluid points embedding microscopic internal degrees of freedom move with the flow field. Some multiscale simulations are similar in the concept to our new method[7, 8]. However, these methods are involved and somewhat cumbersome, since they use the Eulerian and Lagrangian schemes alternatively in their numerical schemes. Our new simulation method is technically simple. By using our method, we can directly trace the material points retaining their strain and strain rate history and easily handle historically dependent fluids.

Here we employ the modified smoothed particle hydrodynamics (MSPH) method[9] as a macroscopic solver. The MSPH method highly improves its accuracy especially at points near the boundary of the domain as compared with the conventional smoothed particle hydrodynamics (SPH) method[10]. As a microscopic polymer simulation, we use the dumbbell model which is the simplest model of polymer in a dilute polymer solution and a standard one as used in CONNFESSIT. An ensemble of the dumbbell model corresponds to an analytical model, e.g. the Maxwell model, and therefore we can verify the validity of our simulation results as a benchmark.

We would like to mention Ellero et al.'s work since the first fully Lagrangian multiscale simulation method has been accomplished by them[11]. In their simulation, the normal SPH method has been employed to solve the macroscopic fluid dynamics. The SPH method fundamentally belongs to a kind of difference methods, therefore the first derivative of arbitrary function is defined between two smoothed particles. However the MSPH method is a variant of least square fitting methods, the derivative is defined just on a corresponding smoothed particle in case of the MSPH method. The MSPH method is rather straightforward to apply to any differential equations than the original SPH method.

The paper is organized as follows. In the next section we explain the multiscale Lagrangian fluid dynamics method. We review the MSPH method and the dumbbell model there. In Section III, the hybrid simulation is applied to study start-up flows in a 2-dimensional channel. Section IV summarizes conclusions.

II. MULTISCALE LAGRANGIAN FLUID DYNAMICS

Cauchy's continuum equation of motion serves as a starting point to consider general fluids:

$$\rho \frac{d\mathbf{v}}{dt} = \nabla \cdot \boldsymbol{\sigma} + \mathbf{f}, \quad (1)$$

where ρ is the density of fluid, \mathbf{v} is the flow velocity, t is time, $\boldsymbol{\sigma}$ is the stress tensor, and \mathbf{f} is the body force. A convective term does not appear in the above equation because we treat fluids here in a Lagrangian manner. The stress tensor $\boldsymbol{\sigma}$ is represented by isotropic pressure p and the deviatoric stress tensor $\boldsymbol{\tau}$:

$$\boldsymbol{\sigma} = -p\mathbf{I} + \boldsymbol{\tau}, \quad (2)$$

where \mathbf{I} is the $d \times d$ identity matrix and d is the dimension of the space. Usually, the pressure p is obtainable because of the incompressibility condition, but the deviatoric stress tensor $\boldsymbol{\tau}$ is not, which arises from microscopic internal degrees of freedom. Since the tensor $\boldsymbol{\tau}$ fully depends on microscopic states, the derivation of the tensor is considerably difficult especially in complex fluid cases such as polymer fluids. Even so, many constitutive relations for the tensor $\boldsymbol{\tau}$ have been found phenomenologically or on the basis of microscopic consideration of polymer chains[12]. They are qualitatively useful in applying to polymer processing, even if they do not hold microscopically detailed structures. Because, these microscopic details are compressed to macroscopic parameters appearing in the constitutive relations.

Polymeric fluids represent stress-strain and stress-strain rate historical dependency coming from microscopic polymer dynamics. The historical dependence of stress is essential in several polymeric phenomena such as strain hardening or shear thinning. In order to handle the effect of microscopic polymer dynamics we need to consider microscopic details omitted in the above constitutive equations. The easiest way to incorporate polymer dynamics is to perform a molecular dynamics simulation of polymers, but such a simulation is impractical to investigate rheological behaviors due to the shortness of computationally accessible time. The other effective simulations have already been developed, and these simulations have been found to represent not only qualitatively but also quantitatively sufficient results[13, 14]. Even so, there is still a gap to apply these simulation methods to polymeric flow problems since they are specialized to find the stress-strain and -strain rate relations in a small simulation box. If we treat such a simulation system so as to give a constitutive

relation under any applied flow, the polymeric flow problems on which microscopic polymer dynamics gives essential influence become solvable by incorporating the microscopic polymer simulation into a fluid dynamics simulation. Such a multiscale simulation method will be available within near future since computer technology is rapidly developing and parallel computing environments become easy to available. Therefore, we are addressing to advance computational techniques to fully utilize the high performance computing technology. The multiscale simulation technique become increasingly important in the future.

In order to develop consistently effective techniques for a future multiscale simulation, first of all, we demand a Lagrangian method to solve fluid dynamics because of its historical dependence coming from the microscopic degrees of freedom. Secondly, highly parallel computing technique is necessary. We present such a multiscale parallel computing technique. We solve start-up flow problems of polymeric fluid in a 2-D channel as a benchmark test in the section III.

A. Macroscopic Fluid Dynamics Simulation

We mentioned the importance of historical dependence of microscopic systems incorporated into the macroscopic system in the previous section. In order to simulate non-Newtonian fluids with a nonlinear relation between shear stress and strain rate, we have to solve the Cauchy's equation of motion in a Lagrangian manner. If we use a Eulerian method to non-Newtonian fluids, we need to consider the convection of the stress from adjacent grids, which means the history of fluids is no longer maintained in the Eulerian manner without introducing auxiliary field such as orientation tensor field and a variable describing the stretch of polymer coils. In some trivial cases such as stationary flows it is easy to obtain the stream line and to know the path through which the fluids flowed in the past. In such cases, we are able to treat the non-Newtonian fluids even in the Eulerian framework by taking into account the convection of the stress[3]. However, their applications are limited to predictable cases. In usage of Lagrangian methods we can treat more general cases.

Before we solve any differential equations, we have to know spatial derivatives of fields, for example $\nabla \cdot \sigma$ appearing in Cauchy's equation of motion. In the Lagrangian picture, the distribution of fluid particles which are used as substitutes for Eulerian grids does not necessarily have a regular pattern and changes momentarily. So it is difficult to define the

derivative values in the Lagrangian frame.

Using some kernel functions to interpolate between the unstructured fluid particles, the SPH method accomplished to obtain average values of the derivatives[10]. Therefore, when we use the SPH method to solve a differential equation, we have to be aware of using the average values. The SPH derives the smoothed derivatives of fields even when the values are drastically changing among fluid particles.

In order to remove the problem mentioned above, we implement the MSPH technique based on the Taylor expansion of the original SPH averages[9]. By using the MSPH method, we are available to obtain first and higher derivatives instead of the averaged derivatives which are given in the original SPH method. Once we calculate the derivative values on a fluid particle, or a calculation point, we have only to substitute them into the differential equations, and then we find their solutions by using a time integrating scheme, for example the velocity Verlet algorithm or the Runge-Kutta method. The MSPH method do not need any alternations of original differential equations, whereas the SPH method demand further considerations because the derivative of fields obtained by using SPH is the average value of the differences defined between fluid particles[11]. The distinction in their treatments results from an approximation accuracy of these methods: The approximation accuracy of SPH is the first order while that of MSPH is the second order.

Here we summarize the MSPH method briefly (see ref.[9] for more information). This method can be regarded as a variant of unstructured grid methods and least square fitting techniques. Based on the SPH procedure, an average of discrete field $f(\mathbf{x}_i)$ on fluid particles \mathbf{x}_i are defined by weighted sum:

$$\langle f(\mathbf{x}_i) \rangle \equiv \sum_j^{\Omega} f(\mathbf{x}_j) W(|\mathbf{x}_i - \mathbf{x}_j|), \quad (3)$$

where $W(x)$ is a Gaussian type function of distance x within a finite region Ω . Originally, field $f(\mathbf{x})$ is continuous, hereafter we use the following continuous representation:

$$\langle f_{\xi} \rangle = \int_{\Omega} d\mathbf{x} f_{\mathbf{x}} W_{\xi\mathbf{x}}, \quad (4)$$

where $f_{\mathbf{x}} \equiv f(\mathbf{x})$ and $W_{\xi\mathbf{x}} \equiv W(|\xi - \mathbf{x}|)$. Then we obtain the following set of equations in

accordance with the usual SPH procedure:

$$\langle f_{\boldsymbol{\xi}} \rangle_{,\alpha} \equiv \langle \nabla_{\alpha} f_{\boldsymbol{\xi}} \rangle = \int_{\Omega} d\mathbf{x} f_{\mathbf{x}} \nabla_{\alpha} W_{\boldsymbol{\xi}\mathbf{x}}, \quad (5a)$$

$$\langle f_{\boldsymbol{\xi}} \rangle_{,\beta\gamma} \equiv \langle \nabla_{\beta} \nabla_{\gamma} f_{\boldsymbol{\xi}} \rangle = \int_{\Omega} d\mathbf{x} f_{\mathbf{x}} \nabla_{\beta} \nabla_{\gamma} W_{\boldsymbol{\xi}\mathbf{x}}, \quad (5b)$$

where $\nabla_{\alpha} X$ denotes a spatial derivative of X with respect to the α -component of $\boldsymbol{\xi}$, i.e. ξ^{α} . We assign coordinate axes to subscript and superscript Greek characters in the present paper. Substituting $f_{\mathbf{x}}$ in the above equations (5) to the following Taylor series of $f_{\mathbf{x}}$ around a reference position $\boldsymbol{\xi}$ represented as

$$\begin{aligned} f_{\mathbf{x}} &= f_{\boldsymbol{\xi}} + (\nabla_{\alpha} f_{\boldsymbol{\xi}})(x^{\alpha} - \xi^{\alpha}) \\ &+ \frac{1}{2}(\nabla_{\beta} \nabla_{\gamma} f_{\boldsymbol{\xi}})(x^{\beta} - \xi^{\beta})(x^{\gamma} - \xi^{\gamma}) + \dots \\ &\equiv f_{\boldsymbol{\xi}} + f_{\boldsymbol{\xi},\alpha} R^{\alpha} + \frac{1}{2} f_{\boldsymbol{\xi},\beta\gamma} R^{\beta} R^{\gamma} + \dots, \quad (R^{\alpha} \equiv x^{\alpha} - \xi^{\alpha}) \end{aligned} \quad (6)$$

the next equations are derived up to the second order in R :

$$\langle f_{\boldsymbol{\xi}} \rangle = f_{\boldsymbol{\xi}} \langle 1 \rangle + f_{\boldsymbol{\xi},\alpha} \langle R^{\alpha} \rangle + \frac{1}{2} f_{\boldsymbol{\xi},\beta\gamma} \langle R^{\beta} R^{\gamma} \rangle, \quad (7a)$$

$$\langle f_{\boldsymbol{\xi}} \rangle_{,\delta} = f_{\boldsymbol{\xi}} \langle 1 \rangle_{,\delta} + f_{\boldsymbol{\xi},\alpha} \langle R^{\alpha} \rangle_{,\delta} + \frac{1}{2} f_{\boldsymbol{\xi},\beta\gamma} \langle R^{\beta} R^{\gamma} \rangle_{,\delta}, \quad (7b)$$

$$\langle f_{\boldsymbol{\xi}} \rangle_{,\epsilon\zeta} = f_{\boldsymbol{\xi}} \langle 1 \rangle_{,\epsilon\zeta} + f_{\boldsymbol{\xi},\alpha} \langle R^{\alpha} \rangle_{,\epsilon\zeta} + \frac{1}{2} f_{\boldsymbol{\xi},\beta\gamma} \langle R^{\beta} R^{\gamma} \rangle_{,\epsilon\zeta}. \quad (7c)$$

We can rewrite these equations (7) to the Matrix form;

$$\begin{pmatrix} \langle f_{\boldsymbol{\xi}} \rangle \\ \langle f_{\boldsymbol{\xi}} \rangle_{,\delta} \\ \langle f_{\boldsymbol{\xi}} \rangle_{,\epsilon\zeta} \end{pmatrix} = \begin{pmatrix} \langle 1 \rangle & \langle R^{\alpha} \rangle & \frac{1}{2} \langle R^{\beta} R^{\gamma} \rangle \\ \langle 1 \rangle_{,\delta} & \langle R^{\alpha} \rangle_{,\delta} & \frac{1}{2} \langle R^{\beta} R^{\gamma} \rangle_{,\delta} \\ \langle 1 \rangle_{,\epsilon\zeta} & \langle R^{\alpha} \rangle_{,\epsilon\zeta} & \frac{1}{2} \langle R^{\beta} R^{\gamma} \rangle_{,\epsilon\zeta} \end{pmatrix} \begin{pmatrix} f_{\boldsymbol{\xi}} \\ f_{\boldsymbol{\xi},\alpha} \\ f_{\boldsymbol{\xi},\beta\gamma} \end{pmatrix}. \quad (8)$$

The number of rows in Eq. (8) is seven in two dimensional space, whereas thirteen in three dimensional space. Considering the commutativity of spatial derivatives ($\nabla_{\alpha} \nabla_{\beta} f = \nabla_{\beta} \nabla_{\alpha} f$), we can reduce the number of rows in Eq. (8) from seven to six in two dimensions because of $f_{\boldsymbol{\xi},yx} = f_{\boldsymbol{\xi},xy}$, and from thirteen to ten in three dimensions;

$$\begin{pmatrix} \langle f_{\boldsymbol{\xi}} \rangle \\ \langle f_{\boldsymbol{\xi}} \rangle_{,\delta} \\ \langle f_{\boldsymbol{\xi}} \rangle_{,\epsilon\zeta} \end{pmatrix} = \begin{pmatrix} \langle 1 \rangle & \langle R^{\alpha} \rangle & C(\beta, \gamma) \langle R^{\beta} R^{\gamma} \rangle \\ \langle 1 \rangle_{,\delta} & \langle R^{\alpha} \rangle_{,\delta} & C(\beta, \gamma) \langle R^{\beta} R^{\gamma} \rangle_{,\delta} \\ \langle 1 \rangle_{,\epsilon\zeta} & \langle R^{\alpha} \rangle_{,\epsilon\zeta} & C(\beta, \gamma) \langle R^{\beta} R^{\gamma} \rangle_{,\epsilon\zeta} \end{pmatrix} \begin{pmatrix} f_{\boldsymbol{\xi}} \\ f_{\boldsymbol{\xi},\alpha} \\ f_{\boldsymbol{\xi},\beta\gamma} \end{pmatrix}. \quad (9)$$

Here we introduce coefficients $C(\beta, \gamma) \equiv 1 - \frac{1}{2} \delta_{\beta\gamma}$ where $\delta_{\beta\gamma}$ is Kronecker's delta.

In order to obtain the differential values $f_{\xi,\alpha} \equiv \nabla_\alpha f_\xi$, our procedure is as follows. At first we calculate the average values $\langle \cdot \rangle$ in Eq. (9) in the usual SPH manner, and then we solve the above linear equation (9) by using, for example, the LU decomposition.

Here, we adopt a Gaussian kernel function $W(x)$ firstly used in the MSPH method[9]:

$$W(x) = \begin{cases} \frac{A_d}{(h\sqrt{\pi})^d} \left(e^{-\frac{x^2}{h^2}} - e^{-4} \right), & \text{if } |x| \leq 2h \\ 0, & \text{otherwise} \end{cases} \quad (10)$$

where d is a dimensionality of the space and the cut-off radius is $2h$. The normalization parameter A_d equals to 1.04823, 1.10081 and 1.18516 for $d = 1, 2$ and 3 , respectively. The density of each distributed particle $\rho(\boldsymbol{\xi})$ is obtained by integrating the kernel function in the same manner as the ordinal SPH method:

$$\rho(\boldsymbol{\xi}) = \int_{\Omega} d\mathbf{x} m W(|\mathbf{x} - \boldsymbol{\xi}|), \quad (11)$$

where m is mass of particle.

As a benchmark of our multiscale simulation, we investigate two types of macroscopic simulation with constitutive relations, Newtonian viscosity model (Newton model) and Maxwell constitutive equation (Maxwell model). Newton model is symbolically represented by a dashpod with a viscosity constant η . The deviatoric stress tensor of Newton model is proportional to strain rate:

$$\boldsymbol{\tau} = 2\eta\mathbf{D} = \eta(\boldsymbol{\kappa} + \boldsymbol{\kappa}^T), \quad (12)$$

where $\boldsymbol{\kappa}$ is velocity gradient tensor defined as $\boldsymbol{\kappa} \equiv \nabla\mathbf{v}$. Maxwell model is symbolically represented by connecting a dashpod with a viscosity constant η and a spring with an elastic constant G in series. Maxwell constitutive equation is expressed as follows:

$$\boldsymbol{\tau} + \lambda\dot{\boldsymbol{\tau}} = 2\eta\mathbf{D}, \quad (13)$$

where λ is a relaxation time. The constants η in Eq. (13) and G are connected through $\eta = G\lambda$.

Assuming the deviatoric stress tensor $\boldsymbol{\tau}$ in the Cauchy's equation of motion (1) as to be Newton model, we obtain the Navier-Stokes equation:

$$\rho \frac{d\mathbf{v}}{dt} = -\nabla p + \eta \nabla^2 \mathbf{v} + \mathbf{f}. \quad (14)$$

Even though we can solve the Navier-Stokes equation directly by using the MSPH method, we elaborately solve the Cauchy's equation of motion (1) after obtaining the deviatoric stress tensor $\boldsymbol{\tau}$ to be applicable to general problems.

We shortly mention how to determine the isotropic pressure p . When we consider high pressure case, e.g. a flow in a duct or shock wave, we can treat an incompressible fluid by solving the Poisson equation of pressure p as shown in Ref. [15]. In low pressure case, the effect of compressibility is negligibly small even if we assume a barotropic fluid $p = p(\rho)$. In this work, we investigate a fluid in low pressure environment only.

We investigate start up flow profiles obtained by solving the Cauchy's equation of motion (1) with two different types of constitutive equations, Newton model (12) and Maxwell model (13). For convenience, we concentrate on the flow behavior between two parallel plates. Assuming translational symmetry for the z -direction which is parallel to plates and perpendicular to the flow direction, we can treat the present system in two dimensional space. At first, we prepare a rectangular system box ($L_x \cdot L_y$) in which particles are regularly displaced as shown in Figure 1. We set the initial distance a between nearest neighbor particles, the mass of particles m and simulation time interval t_0 as unity. The total number of particles N are $L_x \times L_y$. We set the thickness of plates l_w to $3a$ larger than h in order to maintain the density of fluid near the plates as much as that of bulk. We assume the fixed boundary condition for fluid particles on plates and the periodic boundary condition for the x -direction. Applying the body force $\boldsymbol{f} = (1.0 \times 10^{-3}, 0.0) \times m/(a^2 t_0^2)$ to the fluid, the fluid flows toward the x -direction. Values of simulation parameters are summarized in Table I. The displacements of fluid particles are updated according to the following equation after solving the Cauchy's equation of motion (1):

$$\frac{d\boldsymbol{r}}{dt} = \boldsymbol{v}, \quad (15)$$

where \boldsymbol{r} is the position of fluid particle. In order to treat the time-derivative numerically, we discretize it as

$$\frac{df}{dt} \simeq \frac{f^{\text{New}} - f^{\text{Old}}}{\Delta t} \quad (16)$$

with the finite difference $\Delta t = 0.01t_0$. We use the velocity-Verlet algorithm as time-integral scheme.

Figures 2 and 3 represent the flow profiles in cases of Newton model and Maxwell model, respectively. From the positions of tracer particles we can extract their characters of flow

behaviors. In case of Newton model, flow profiles show a plane Poiseuille flow, however, those of Maxwell model represent a plug flow like behavior when the elastic constant is very small and the relaxation time is very long. Maxwell model (13) corresponds to Newton model (12) in the limit $\lambda\dot{\boldsymbol{\tau}} \rightarrow 0$, while keeping η constant, which means that the elastic property of the spring can be negligible. Therefore, when the relaxation time λ becomes smaller, the flow behavior of Maxwell model approaches to that of Newton model.

B. Microscopic Polymer Simulation

In this study, we select the dumbbell model as microscopic model of polymer in our multiscale simulation since the dumbbell model is the simplest and in the statistical limit it corresponds to an analytical model, i.e. the Maxwell model. The dumbbell model is modeling a dilute polymeric fluid without entanglements between polymers. The dynamics of a dumbbell consists of elastic dynamics and thermal fluctuation.

$$\begin{aligned}\Delta\mathbf{Q} &\equiv \mathbf{Q}(t + \Delta t) - \mathbf{Q}(t) \\ &= \left(\boldsymbol{\kappa} \cdot \mathbf{Q} - \frac{1}{2\lambda}\mathbf{Q} \right) \Delta t + \sqrt{\frac{\Delta t}{\lambda}}\boldsymbol{\Phi},\end{aligned}\tag{17}$$

where \mathbf{Q} is end-to-end vector of the dumbbell, and $\boldsymbol{\Phi}$ is the Gaussian white noise that is satisfying the following equations:

$$\langle \boldsymbol{\Phi}(t) \rangle = 0,\tag{18a}$$

$$\langle \Phi_\alpha(t)\Phi_\beta(t') \rangle = \delta_{\alpha\beta}\delta(t - t').\tag{18b}$$

We can derive the expression for the dumbbell model (17) from microscopic view points[16, 17]. For simplicity, we only explain about the roles of each term here. The parentheses of the first term in Eq. (17) consists of Affine deformation and elastic dynamics. The relaxation time λ is related to the elastic constant G as discussed in the previous subsection. When the relaxation time of dumbbell is large, the dumbbell is easy to be extended since the elastic constant $G = \eta/\lambda$ is small. The relaxation time of dumbbell also appears in the coefficient of second term in the right-hand-side of Eq. (17) through the fluctuation-dissipation theorem. The dumbbell with a long relaxation time is sensitive to the Affine deformation rather than the elastic relaxation and the thermal fluctuation. The averaged stress in a microscopic

simulation system is represented by Kramers-Kirkwood formula:

$$\boldsymbol{\tau} = G(\langle \mathbf{Q}\mathbf{Q} \rangle - \mathbf{I}). \quad (19)$$

Generally speaking, the Kramers-Kirkwood formula consists of contributions from a solvent, intramolecular forces, external forces, dynamics of beads, and isotropic pressure[2]. To simplify our arguments, we only consider the effects of intramolecular forces and isotropic pressure in Eq. (19). This lead us to concentrate on the orientation and length of end-to-end vector of dumbbell.

To update the end-to-end vector according to Eq. (17), we adopt the second order stochastic Runge-Kutta algorithm here[18]. This algorithm decreases order of numerical errors from $O((\Delta t)^2)$ contained in ordinary Brownian dynamics algorithms to $O((\Delta t)^3)$. These errors are caused by its numerical algorithm not by the random noise. Initial conditions of dumbbells are prepared by performing the dumbbell simulation under a stationary condition over twice of the relaxation time.

Figure 4 shows the stress history under a constant shear rate $\kappa = 1.0/t_0$ with $\lambda = 100t_0$ and $G = 0.01m/a$ comparing the dumbbell model and Maxwell model. The thermal fluctuation appears after the Newtonian viscosity $\eta = \tau/\kappa$ grows up to the zero shear viscosity, however it doesn't appear or negligibly small in the transient region. This stress history process can be separated into two processes, elongation and rotation of dumbbells, respectively. The border line exists at more or less $t/\lambda = 1$. The stress tensor (19) is insensitive to the effect of random noise in the elongation process, since the orientations of dumbbells are almost same direction. In the rotation process, however, the angular velocity of dumbbells is sensitive to the length of end-to-end vector, and therefore the thermal fluctuation becomes influential. Increasing the number of dumbbells N_d , the fluctuation of stress is decreasing in proportional to $N_d^{-1/2}$ by the law of large numbers in statistics because the stress is defined by a statistical average of $G(\mathbf{Q}\mathbf{Q} - \mathbf{I})$ over N_d dumbbells as shown in Eq. (19). We expect the dumbbell model corresponds to Maxwell model in the limit $N_d \rightarrow \infty$. As shown in Fig. 4, the thermal fluctuation has been almost suppressed when $N_d = 10000$.

C. Macro-micro Hybridization

In the previous subsections II A and II B, we have introduced the simulation techniques of macroscopic fluid dynamics and microscopic polymer dynamics and explained about their features. Now we incorporate them in order to treat polymeric fluid dynamics. The main idea of our hybrid simulation is similar to that of CONNFFESSIT; we perform the polymer simulation in stead of the constitutive equation in order to obtain the stress tensor σ in Cauchy's equation of motion (1).

The procedure of our simulation is summarized to the following steps:

1. Macroscopic fluid dynamics simulation to update \mathbf{r} , \mathbf{v} , and p .
2. MSPH method to obtain $\nabla\mathbf{v}$.
3. Microscopic polymer simulation to update τ .
4. MSPH method to obtain $\nabla \cdot \sigma$.
5. Return to 1.

We perform these processes every time steps. We adopt the linked list algorithm[19] to find a pair of particles at macroscopic fluid simulation in order to decrease the calculation time $O(N^2)$ to $O(N)$ for N particles. In each step, we can perform the calculations on a particle independently from those of other particles, and therefore we benefit from usage of parallel computing.

III. NUMERICAL RESULTS ON HYBRID SIMULATION

Now we investigate the flow profiles of multiscale Lagrangian fluid dynamics simulation and compare the resultant flow profiles with the macroscopic results shown in Sec. II A. We perform the multiscale simulation under the same condition explained in Sec. II A, however we use the dumbbell model to obtain the deviatoric stress tensor τ . We set the number of dumbbells N_d in each fluid particle to 1000. Under the environment using 2×3.16 GHz Quad-Core Intel Xeon processor (8 cores) and OpenMP (Open Multi-Processing) programming interface, the calculation time for 100 cycles of the simulation procedure explained in the

previous section II C is about 2.5 minutes, which corresponds to $t = 1.0t_0$ because of $\Delta t = 0.01t_0$.

Figure 5 represents the flow behaviors obtained from our new simulation technique. Comparing between Figs. 3 and 5, the tendencies of these flows are almost similar, except for the thermal fluctuation observed in Fig. 5. When the relaxation time λ is small, the fluctuation of fluid becomes larger. There are two reasons. One reason is that the coefficient of random noise in Eq. (17) is large in λ small case, because of the fluctuation dissipation theorem. Another one is that time of elongation process, discussed in Sec. II B, becomes short, and then the thermal fluctuation appears earlier.

We have also performed the multiscale simulation with $N_d = 10000$. The resultant flow behaviors have been very close to those of the Maxwell model which are shown in Fig. 3, since the thermal fluctuation in this case has been almost suppressed as mentioned in Sec. II B.

Strictly speaking, the incompressibility doesn't satisfied at some local regions in the present simulation. In order to improve this failure, we should solve the Poisson equation of isotropic pressure p [15].

IV. CONCLUSION

We have developed the multiscale Lagrangian fluid dynamics technique to simulate a hierarchical polymeric fluid where the stress on each particle consisting of a large number of molecules depends on history of shear strain and/or shear rate. We have investigated the simplest case of polymeric flow problems, and then obtained the desirable results.

Our multiscale simulation has extensibilities to deal with more complex phenomena on polymeric fluid by upgrading the dumbbell model to either a direct polymer simulation such as the Kremer-Grest model[20] or a more effective model to introduce the idea of polymer reptation and entanglements such as the slip-link model[13] and the primitive chain network model[14]. Our application to flow problems on complex boundaries, e.g. contraction/expansion flow or free boundary flow, can be straightforward. Microscopic level simulations are independent of others, and therefore they can be highly parallelized.

Although we referred only to polymeric fluids in the present paper, our multiscale approach can be applied to general flow problems, e.g. granular materials and powder systems,

only if the density of materials is sufficiently uniform in the macroscopic scale in the framework of this paper. When we apply our multiscale simulation to nonuniform density case, we need to delete the incompressibility condition at macroscopic level, and we should consider the grand canonical ensemble at microscopic level simulations in order to exchange microscopic internal freedom degrees among macroscopic particles.

Acknowledgements

We would like to thank all members in the group of *Multiscale Simulation for Softmatters* for their advices and fruitful discussions. This research was supported by *Core Research for Evolutional Science and Technology (CREST) of Japan Science and Technology Agency Corporation (JST)*.

-
- [1] Boger, D. V.; Walters, K. Rheological phenomena in focus; Elsevier: Amsterdam ; London, 1993.
 - [2] Bird, R. B.; Armstrong, R. C.; Hassager, O. Dynamics of polymeric liquids; Wiley: New York ; Chichester, 1987.
 - [3] Laso, M.; Öttinger, H. JOURNAL OF NON-NEWTONIAN FLUID MECHANICS 1993, 47, 1-20.
 - [4] Phillips, T.; Williams, A. JOURNAL OF NON-NEWTONIAN FLUID MECHANICS 1999, 87, 215-246.
 - [5] Ren, W.; Vanden-Eijnden, E.; Maragakis, P.; E, W. JOURNAL OF CHEMICAL PHYSICS 2005, 123, 134109.
 - [6] Yasuda, S.; Yamamoto, R. PHYSICS OF FLUIDS 2008, 20, 113101.
 - [7] Laso, M.; Picasso, M.; Ottinger, H. AICHE JOURNAL 1997, 43, 877-892.
 - [8] Halin, P.; Lielens, G.; Keunings, R.; Legat, V. JOURNAL OF NON-NEWTONIAN FLUID MECHANICS 1998, 79, 387-403.
 - [9] Zhang, G.; Batra, R. COMPUTATIONAL MECHANICS 2004, 34, 137-146.
 - [10] Monaghan, J. REPORTS ON PROGRESS IN PHYSICS 2005, 68, 1703-1759.
 - [11] Ellero, M.; Espanol, P.; Flekkoy, E. PHYSICAL REVIEW E 2003, 68, 041504.

- [12] Doi, M.; Edwards, S. F. The theory of polymer dynamics; Clarendon Press: Oxford, 1986.
- [13] Shanbhag, S.; Larson, R.; Takimoto, J.; Doi, M. PHYSICAL REVIEW LETTERS 2001, 87, 195502.
- [14] Masubuchi, Y.; Takimoto, J.; Koyama, K.; Ianniruberto, G.; Marrucci, G.; Greco, F. JOURNAL OF CHEMICAL PHYSICS 2001, 115, 4387-4394.
- [15] Koshizuka, S.; Oka, Y. NUCLEAR SCIENCE AND ENGINEERING 1996, 123, 421-434.
- [16] Öttinger, H. C. Stochastic processes in polymeric fluids : tools and examples for developing simulation algorithms; Springer: Berlin ; New York, 1996.
- [17] Larson, R. G. The structure and rheology of complex fluids; Oxford University Press: New York ; Oxford, 1999.
- [18] Branka, A.; Heyes, D. PHYSICAL REVIEW E 1998, 58, 2611-2615.
- [19] Rapaport, D. C. The art of molecular dynamics simulation; Cambridge University Press: Cambridge, 2003.
- [20] Kremer, K.; Grest, G. JOURNAL OF CHEMICAL PHYSICS 1990, 92, 5057-5086.

TABLE I: Fixed parameter values in this paper.

t_0	1.0 [T]
a	1.0 [L]
m	1.0 [M]
η	$m/(at_0)$
Δt	$1.0 \times 10^{-2}t_0$
ρ_0	m/a^3
(L_x, L_y)	$(20a, 30a)$
N	600
h	$2a$
l_w	$3a$
\mathbf{f}	$(1.0 \times 10^{-3}, 0.0) \times m/(a^2t_0^2)$

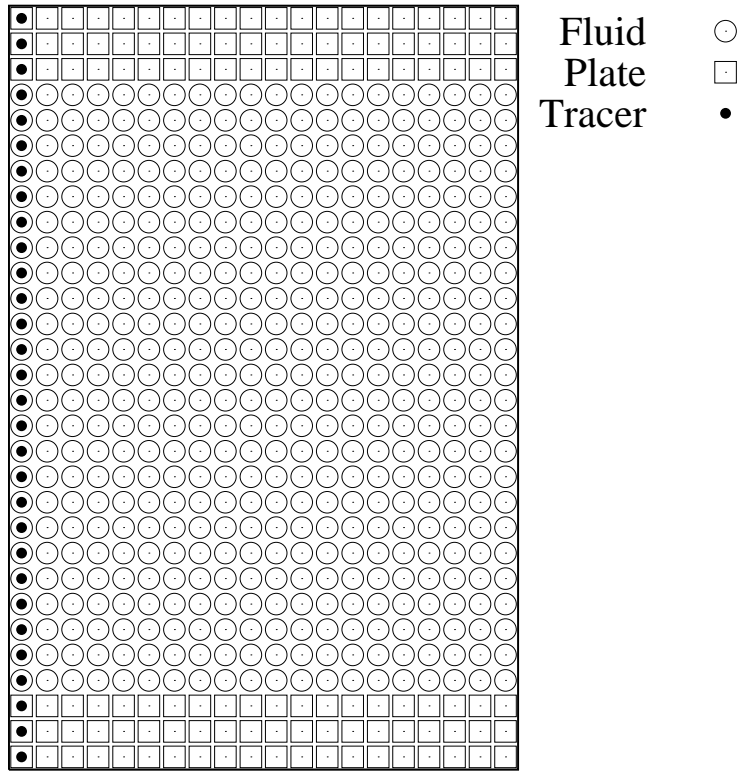


FIG. 1: Initial configuration for Lagrangian fluid simulation.

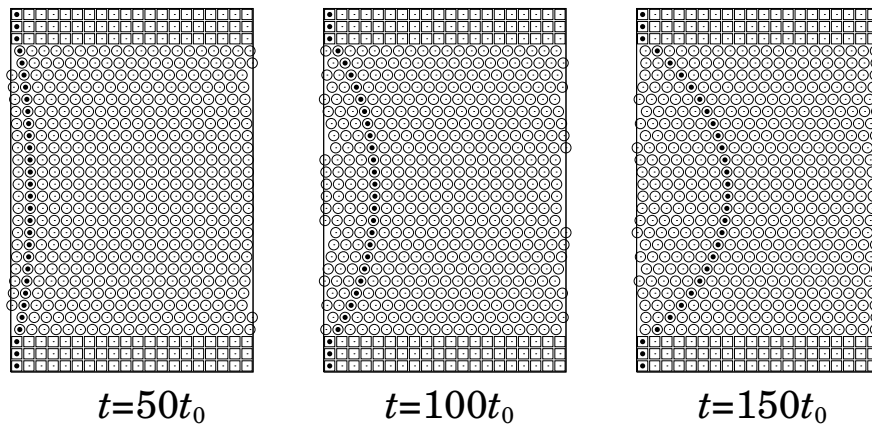


FIG. 2: Profiles of Newtonian flow ($t = 50t_0, 100t_0, 150t_0$).

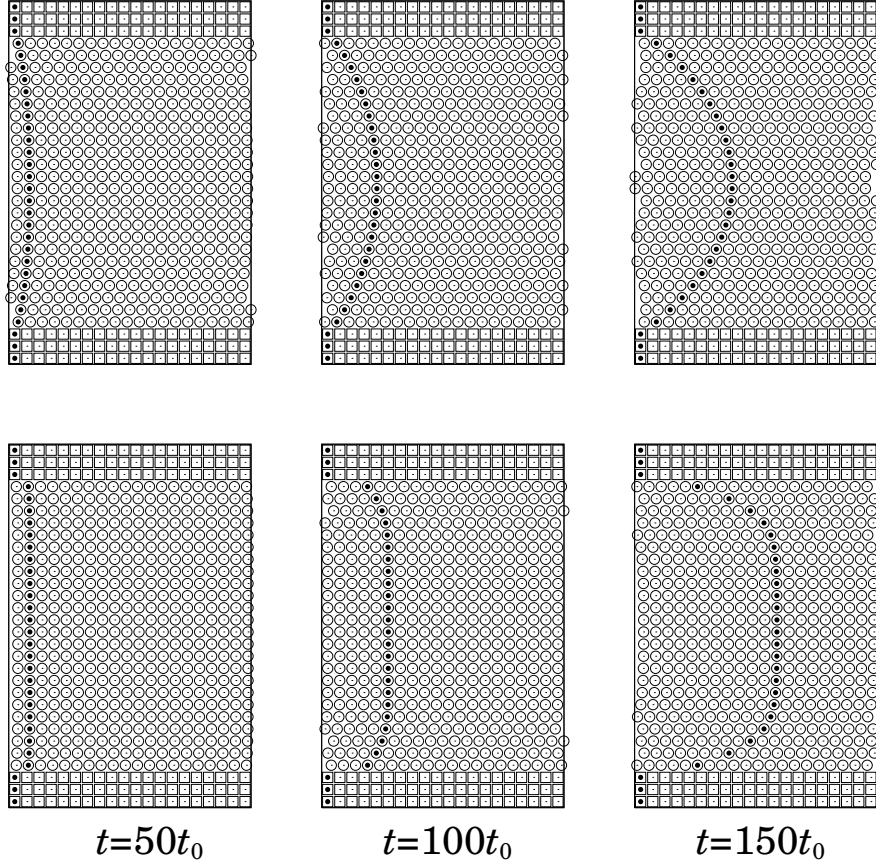


FIG. 3: Flow profiles in case of Maxwell model ($t = 50t_0, 100t_0, 150t_0$) with $\lambda = 10.0t_0$ and $G = 0.1m/a$ (upper group), or $\lambda = 1000t_0$ and $G = 0.001m/a$ (lower group). In both cases, $\eta = G\lambda = 1.0m/(at_0)$.

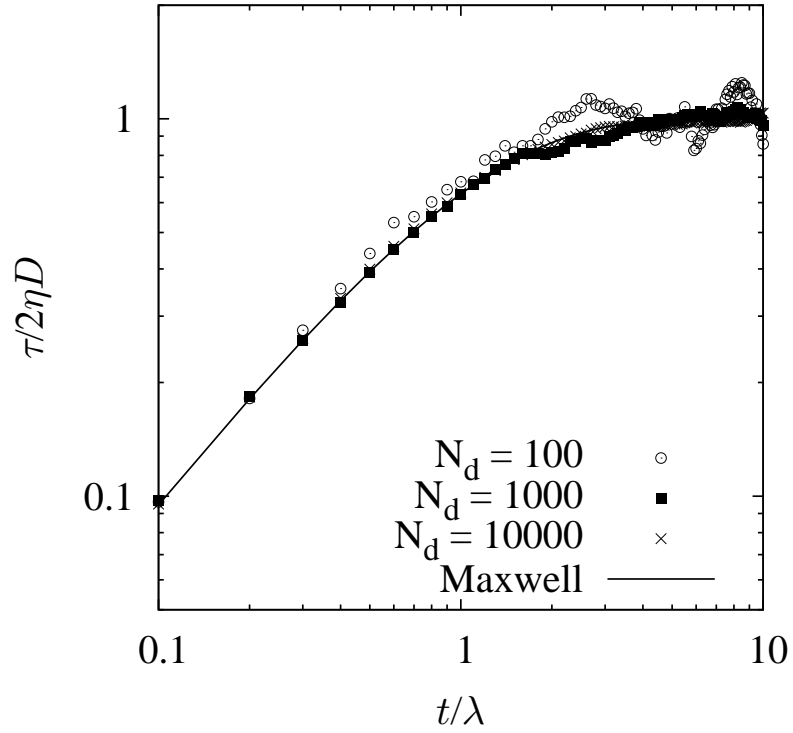


FIG. 4: The stress histories under the constant shear rate $\kappa = 1.0/t_0$ for the systems consists of the dumbbells with $N_d = 100$, $N_d = 1000$, and $N_d = 10000$, and for the Maxwell constitutive equation. The thermal fluctuation depends on the number of dumbbells.

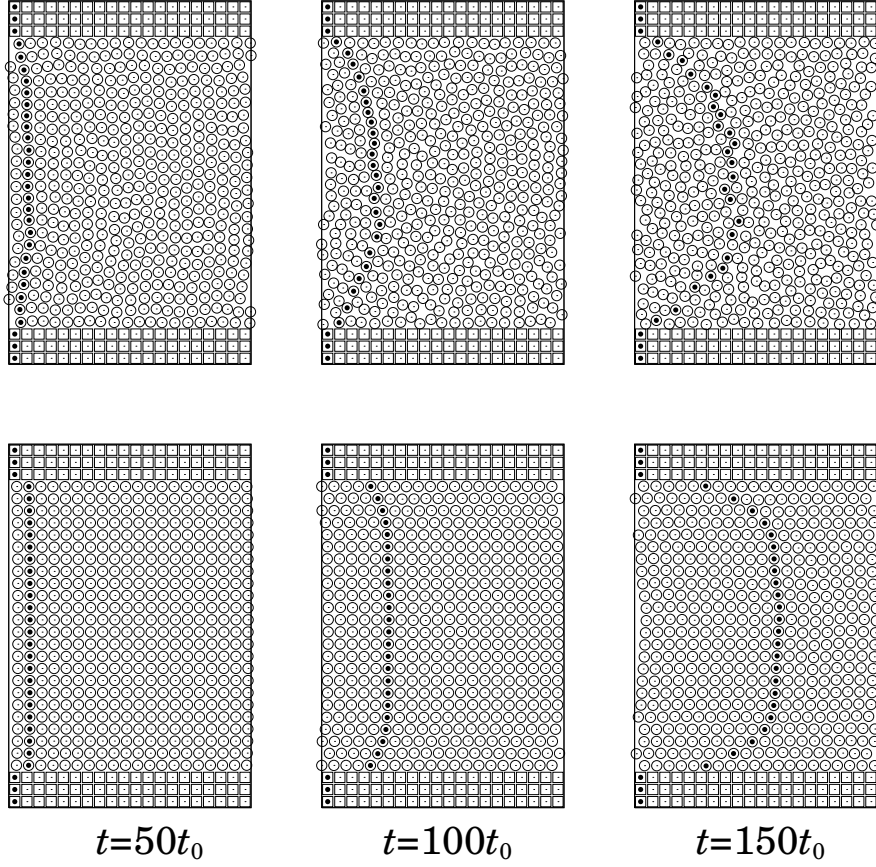


FIG. 5: Flow profiles obtained by performing multiscale Lagrangian fluid dynamics ($t = 50t_0, 100t_0, 150t_0$) with $\lambda = 10.0t_0$ and $G = 0.1m/a$ (upper group), or $\lambda = 1000t_0$ and $G = 0.001m/a$ (lower group). Each fluid particle has 1000 dumbbells instead of Maxwell model.